# Composite Films of Poly(3-hexylthiophene) Grafted Single-Walled Carbon Nanotubes for Electrochemical Detection of Metal Ions

Shaojun Yang,[†,‡,#] Dongli Meng,[†,#] Jinhua Sun,[†] Yan Huang,[‡] Yong Huang,[†] and Jianxin Geng[*,†]

[†]Technical Institute of Physics and Chemistry, Chinese Academy of Sciences, 29 Zhongguancun East Road, Haidian District, Beijing 100190, China

[‡]Key Laboratory of Oil & Gas Fine Chemicals, Ministry of Education & Xinjiang Uyghur Autonomous Region, Xinjiang University, Urumqi 830046, China

**S** *Supporting Information*

**ABSTRACT:** In this study, we prepared electrochemically active films of poly(3-hexylthiophene) grafted single-walled carbon nanotubes (SWNT-g-P3HT) by using a modified vacuum-assisted deposition approach, in which a SWNT-g-P3HT composite layer of various thicknesses was deposited on the top of a thin SWNT layer. Measurement of the optical and electrical properties of the SWNT-g-P3HT composite films demonstrated that the thickness of the SWNT-g-P3HT composite films was controllable. The data of transmission electron microscope observation and Raman spectroscopy indicated that the covalent grafting of P3HT onto the surfaces



of SWNTs resulted in intimate and stable connectivity between the two components in the SWNT-g-P3HT composite. Capitalizing on these unique features, we successfully developed a new class of electrochemical sensors that used the SWNT-g-P3HT composite films deposited on an indium−tin oxide substrate as an electrochemical electrode for detection of metal ions. Significantly, such a SWNT-g-P3HT composite electrode showed advantages in selective, quantitative, and more sensitive detection of Ag^{+} ions.

**KEYWORDS:** *SWNTs, P3HT, composites, films, detection, ions*
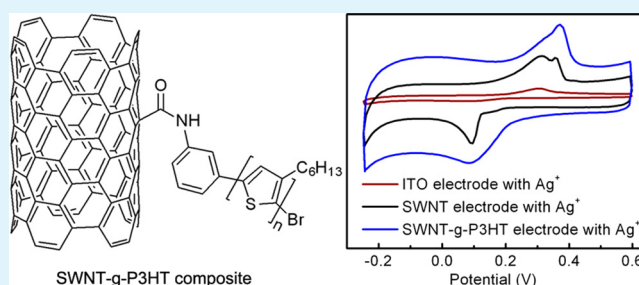
## ■ INTRODUCTION

Thin films of single-walled carbon nanotubes (SWNTs) have attracted enormous attention among scientists due to their widespread applications in areas such as transparent electrodes,[1,2] thin film transistors (TFTs),[3−5] and biological and chemical sensors.[6−8] For the films of these applications, they are commonly prepared by spray coating,[7,9] vacuum-assisted deposition,[10] stamping and printing methods.[5,6] The performance of the films is strongly dependent on the material properties such as purity, metallity, dispersibility, and doping state. For example, the use of SWNT films that comprise of semiconductor-enriched SWNTs presents a highly promising approach for preparation of high performance TFTs,[11−13] while metallic-enriched SWNT samples give rise to higher conductivity of the corresponding SWNT films.[14−16] Acid treatment of the SWNT films, which enhances the contacts between the SWNTs by removing the surfactant from their surfaces,[17] and transition metal doping,[18] which introduces doping effects and ohmic contacts between the semiconductor- and metallic-SWNT networks, also improve the electrical conductivity of the transparent conductive SWNT films.

Surface functionalization of SWNTs with conjugated polymers represents an important approach for improving the proccessability of SWNTs, which also incorporates the attributes of the two components such as conducting properties

and optical properties into the resultant composites. Non-covalent strategy can effectively reserve the conjugated surfaces of SWNTs, whereas the interfaces between SWNTs and conjugated polymers may not be sufficiently intimated for efficient charge transfer for optoelectronic applications.[19] In fact, the noncovalent interactions between SWNTs and conjugated polymers also depend on the main-chain structure of the conjugated polymers.[20−22] Recently, conjugated block copolymers have been demonstrated to be efficient to solubilize SWNTs, where the conjugated fragment provides efficient interface interactions with SWNTs and the nonconjugated fragment facilitates the dispersion of the composite in organic solvents.[23−25] On the other hand, covalently grafting conjugated polymers onto the surfaces of SWNTs leads to more intimated and stabilized connectivity between the two components, resulting in strong electronic interactions.[26] Our previous results indicated that the structural defects on the surfaces of SWNTs interfere with the electron transfer properties in the SWNT/poly(3-hexylthiophene) (P3HT) hybrid materials.[27] In addition, the incorporation of SWNTs into P3HT provides optimized morphology of the SWNT/

P3HT composite films and enhanced crystallinity of the P3HT component in the composite films, as well as a continuous pathway for dissociated charge carriers, thereby leading to enhanced solar cell performance.[28]

The thin films of SWNT/conjugated polymer composites, including both noncovalently and covalently hybridized types, show widespread applications in polymer photovoltaics,[26,28] sensors,[29,30] organic TFTs,[19,24,31] photo- or electroresponsive devices,[32−34] and polymer electroluminescence devices.[25] Such composite films usually share one feature: the conjugated polymers account for the dominated component in the composite films. Various methodologies such as spin coating,[24,25,33] layer-by-layer assembly,[32,35,36] and electropolymerization[37,38] have been developed for preparing large-sized SWNT/conjugated polymer composite films that contain a dominated component of conjugated polymers. A small amount of SWNTs in the conjugated polymer matrix can significantly enhance the performance of the resultant devices. On the other hand, in order to emphasize the feature of carbon nanotubes such as electrical conductivity, it is required to prepare SWNT/conjugated polymer composite films in which SWNTs are a dominated component and the connectivity between the two components is intimate and stable. However, preparation of such large-sized SWNT/conjugated polymer composite films has still rarely reported.

In this work, we covalently grafted P3HT onto the surfaces of SWNTs (SWNT-g-P3HT) and prepared SWNT-g-P3HT composite films by using a modified vacuum-assisted deposition approach, where a thin SWNT film was used as a supporting layer and the SWNT-g-P3HT composite layer of various thicknesses was deposited on the top of the SWNT layer. The morphology, structure, and electrical properties of the films were studied. Significantly, the SWNT-g-P3HT composite films prepared on an indium−tin oxide (ITO) substrate demonstrate application as an electrochemical electrode for selective detection of Ag$^+$ ions.

## ■ EXPERIMENTAL SECTION

**Materials.** The SWNTs used in this study were prepared by the hydrogen arc discharge method,[39] and purified by dry oxidization at 300 °C for 60 min in a flow of dry air (0.1 SLM) and washing in 12 M HCl solution.[40] All the inorganic salts (extra purity grade) were purchased from Sinopharm Chemical Co. Ltd.

**Synthesis of P3HT.** Amino-terminated P3HT (P3HT-NH$_2$) was polymerized through the Grignard metathesis (GRIM) reaction,[41] which is a universal method for synthesis of conjugated polymers with narrow molecular weight distribution and high regularity. The amine groups were incorporated into the polymer chains by ending the polymerization using a proper Grignard reagent (see Figure S1, Supporting Information). The number-averaged molecular weight of the P3HT-NH$_2$ was ca. 3200, as determined by gel permeation chromatography using a polystyrene standard.

**Synthesis of SWNT-g-P3HT Composite.** To graft P3HT onto the surfaces of SWNTs, the purified SWNTs were first oxidized by using nitric acid to produce carboxyl groups. In a typical reaction, purified SWNTs (150 mg) were dispersed in a 3 M HNO$_3$ solution (150 mL) with the aid of sonication for 2 h, followed by refluxing at 120 °C for 48 h. After that, the reaction solution was again sonicated for 1 h and refluxed for 48 h. Finally, the oxidized SWNTs was obtained by vacuum filtration, redispersing in 1 M HCl solution (30 mL), washing with deionized (DI) water, and drying in a vacuum oven at 60 °C overnight.

P3HT was grafted on the surfaces of SWNTs by amidation reaction. Briefly, the oxidized SWNTs (30 mg) were dispersed in DMF (10 mL) under sonication for 3 h. After addition of SOCl$_2$ (30 mL), the reaction mixture was refluxed at 70 °C for 24 h. The acyl chloride activated SWNTs (SWNTs-COCl) were obtained by centrifuging and washed by cycles of dispersing the SWNTs-COCl in anhydrous tetrahydrofuran (THF) and centrifuging. To carry out the amidation reaction, the SWNTs-COCl suspension in anhydrous THF (30 mL) was added into a P3HT-NH$_2$ solution in anhydrous THF (P3HT-NH$_2$ 200 mg, THF 50 mL), followed by droplet addition of triethylamine (3 mL) at 0 °C. The reaction was allowed to carry out at room temperature for 9 h and 50 °C for 48 h. Finally, the SWNT-g-P3HT composite was obtained by centrifuging, and the ungrafted P3HT was removed by cycles of redispersing the product in THF and centrifuging.

**Preparation of SWNT-g-P3HT Composite Films.** SWNT-g-P3HT composite films were prepared by using the vacuum filtration method.[42,43] To obtain SWNT-g-P3HT composite films with high strength, the vacuum filtration method was modified: a thin layer of SWNTs was first deposited on the surface of a anodic aluminum oxide (AAO) membrane, and then the SWNT-g-P3HT composite layer of various thicknesses was deposited on the top of the SWNT layer. AAO membranes with 47 mm diameter and 0.1 μm pores were used.

A SWNT suspension was prepared by dispersing the purified SWNTs (9 mg) in a sodium dodecyl sulfonate (SDS) aqueous solution (30 mL, 3 mg·mL$^{-1}$) by sonication for 10 h. The SWNT suspension was subjected to centrifuge at 10 000 rpm for 10 min to remove the bundled SWNTs, and the supernatant was collected for preparing the supporting SWNT layer. The concentration of the SWNT suspension was determined to be 31 mg·L$^{-1}$ by comparing its extinction coefficient with the reported value.[44] The SWNT-g-P3HT composite was dispersed in THF. The concentration of the composite suspension was calibrated by using UV−visible spectra: the concentration was adjusted to obtain a same absorbance value at 710 nm as that of the SWNTs suspension. The absorbance value at 710 nm was used because P3HT does not show any absorption at this wavelength so that the two suspensions had the same concentration of SWNTs.

The SWNT-g-P3HT composite films on AAO membranes were dried in a 60 °C oven overnight. After that, the AAO membranes were put on the surface of a NaOH solution (3 M) to dissolve the AAO, leading to deposition of the SWNT-g-P3HT composite films on the surfaces of the NaOH solution. After the NaOH solution was thoroughly exchanged with DI water, the SWNT-g-P3HT composite films were deposited on substrates such as ITO, glass, and quartz. Finally, the SWNT-g-P3HT composite films were dried in a 60 °C oven overnight.

**Characterization.** Fourier transform infrared spectroscopy (FT-IR) spectra were recorded on an Excalibur 3100 spectrometer with a resolution of 0.2 cm$^{-1}$ using KBr pellets. Raman spectra were collected on a Renishaw inVia-Reflex confocal Raman microscope with an excitation wavelength of 532 nm. UV−visible spectra of the films were recorded with on a Cary 5000 UV−vis-NIR spectrometer. Photoluminescence (PL) spectra were collected on a Hitachi F-4600 spectrophotometer. Thermogravimetric analysis (TGA) was performed with a Q50 TGA at a scanning rate of 5 °C·min$^{-1}$ under the protection of N$_2$. Transmission electron microscopy (TEM) observations were performed on a JEOL JEM-2100 TEM operated at 200 kV. TEM samples were prepared by dropping the SWNT suspension in SDS solution or the SWNT-g-P3HT composite suspension in THF on 400-mesh Cu grids with supporting carbon films. Scanning electron microscopy (SEM) observations were performed on a Hitachi S4300 field emission scanning electron microscope operated at an acceleration voltage of 10 kV. Sheet resistance of the films was obtained from the slope of the I−V curves obtained on Keithley 4200-SCS, as the areas between the two electrodes were squares. Electrochemical impedance spectroscopy (EIS) and cyclic voltammetry (CV) curves were collected on a Zennium 40088 electrochemical workstation. The SWNT films and the SWNT-g-P3HT composite films used for electrochemical detection were prepared on ITO substrate and they had a size of ca. 1 cm$^2$. In the electrochemical characterization, KNO$_3$ (0.2 M) was used as a supporting electrolyte.

7687

dx.doi.org/10.1021/am500973m | ACS Appl. Mater. Interfaces 2014, 6, 7686−7694

**Scheme 1. Reaction Route for Synthesizing the SWNT-g-P3HT Composite**
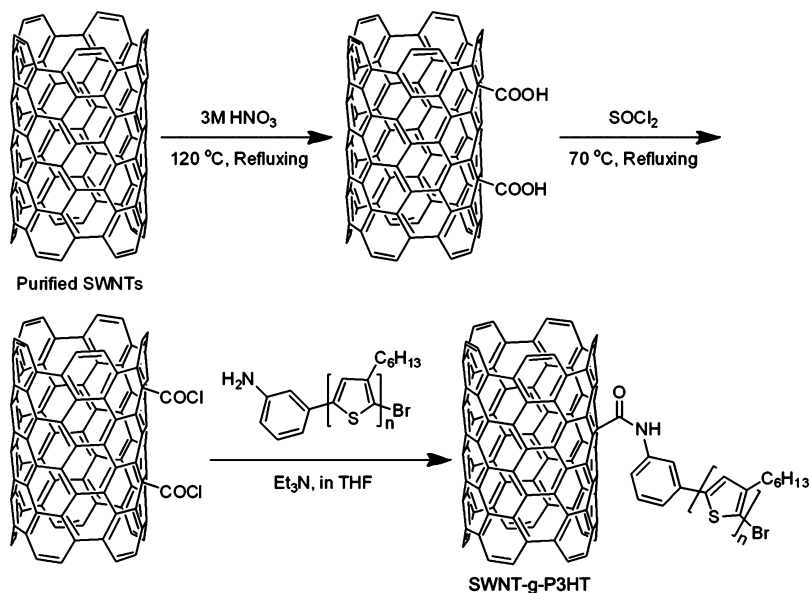


## ■ RESULTS AND DISCUSSION

Scheme 1 represents the procedure of grafting P3HT on the surfaces of SWNTs, which includes generation of carboxyl acid groups on the surfaces of SWNTs through $HNO_3$ oxidation and the amidation reaction of the carboxyl groups with the amine groups of the P3HT-$NH_2$. The product of each reaction was confirmed by using FT-IR spectroscopy (Figure S2, Supporting Information). As proved in a previous study,[26] the SWNT-g-P3HT composite showed enhanced dispersibility in common solvents such as chloroform, THF, chlorobenzene, and dichlorobenzene.

The thermal stability and composition of the SWNT-g-P3HT composite were evaluated by using TGA (Figure 1a). Purified SWNTs are extremely stable, as there is no obvious mass loss up to 900 °C. P3HT shows an obvious mass loss from 300 to 500 °C. As expected, the SWNT-g-P3HT composite exhibits the combined features of P3HT and SWNTs. One can see a mass loss from 300 to 500 °C, corresponding to the thermal degradation of P3HT, which is followed by a thermal stable period up to 900 °C. The differential TGA curves provide more details about the thermal degradation for each component in the composite (Figure S3, Supporting Information). Collectively, the grafting content of P3HT on the surfaces of SWNTs was calculated to be ca. 7.2% in the composite, i.e., ca. 3400 C atoms of SWNTs correspond to one P3HT chain. Furthermore, the grafted P3HT on the surfaces of SWNTs was also confirmed by using TEM. The bundles of purified SWNTs have relatively clear surfaces even at a high magnification (Figure 1b), whereas P3HT bumps can be seen attaching on the surfaces of the bundles of the SWNT-g-P3HT composite (Figure 1c). Because the SWNT-g-P3HT composite was repeatedly washed with THF during purification, the P3HT bumps must be covalently attached on the surfaces of SWNTs.

The interface interactions between SWNTs and P3HT in the SWNT-g-P3HT composite were further characterized by using Raman spectroscopy (Figure 2). Purified SWNTs yield a Raman spectrum that contains a sharp G band peak at 1583 $cm^{-1}$ and a weak D band peak at ca. 1350 $cm^{-1}$. The D band indicates the existence of structural defects on the surfaces of

SWNTs. Upon treatment in $HNO_3$, the oxidized SWNTs show an enhanced D band and a high-frequency shifted G band (at 1602 $cm^{-1}$) due to the oxidized surfaces. P3HT exhibits a Raman spectrum containing a strong sharp peak at 1445 $cm^{-1}$ and a weak sharp peak at 1379 $cm^{-1}$, which are contributed to the C–C skeletal stretching vibration and the C=C skeletal stretching vibration.[45,46] As expected, the Raman spectrum of the SWNT-g-P3HT composite exhibits the information on both SWNTs and P3HT. In addition to that, the G band of SWNT component shifts to a low-frequency position (at 1580 $cm^{-1}$) compared to that of purified SWNTs and oxidized SWNTs. This phenomenon could be interpreted as electron transfer between P3HT and SWNTs.[46] The tail on the left side of the peak at 1379 $cm^{-1}$ is ascribed to the overlapping of P3HT's Raman band (corresponding to the C=C skeletal stretching vibration) and SWNTs' D band.[46] As a result, the Raman data demonstrate intimate interactions between SWNTs and P3HT in the SWNT-g-P3HT composite.

The vacuum-assisted deposition technique is a widely used method for preparing thin films of carbon materials such carbon nanotubes and graphene.[10,42,43] The prepared SWNT films are extremely robust because of the strong intermolecular interactions between the nanotubes. Our experience has proved that the SWNT films can be endurable to ultrasonication. In this research, we tried to prepare SWNT-g-P3HT composite films by directly depositing the SWNT-g-P3HT composite through vacuum filtration. However, the composite films were likely to break in the process of transferring them onto a substrate. This might be due to the P3HT grafted on the surfaces of SWNTs, which weakens the intermolecular interactions between SWNTs. To solve this problem, we used a very thin layer of SWNTs to support the SWNT-g-P3HT composite layer. Because we use the electrochemical properties of the SWNT-g-P3HT composite films as discussed below, the film configuration with a very thin SWNT layer buried inside the films and the SWNT-g-P3HT composite making the outer layer of the films will not handicap the application of the SWNT-g-P3HT composite.

A thin SWNT film was first prepared by using 0.4 mL of the purified SWNT suspension (31 mg·L$^{-1}$ in a SDS aqueous
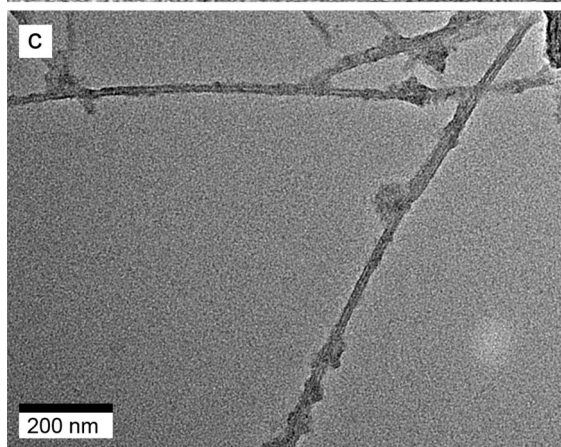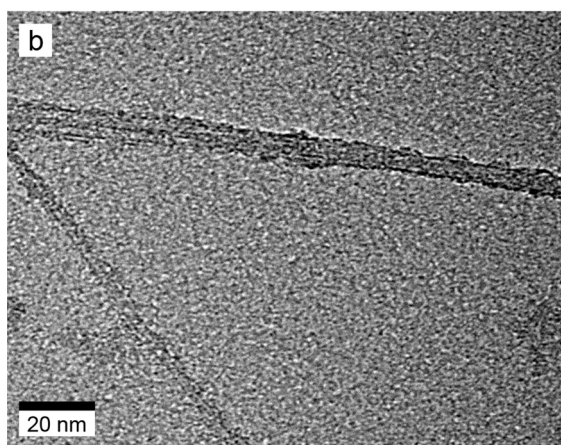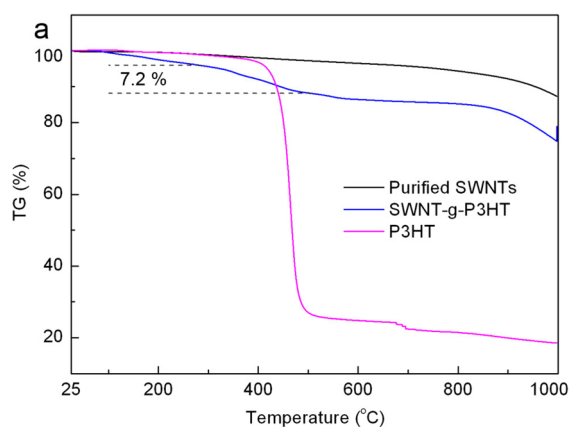
**Figure 1.** (a) TGA curves of purified SWNTs, P3HT, and the SWNT-g-P3HT composite, (b, c) TEM images of (b) oxidized SWNTs and (c) the SWNT-g-P3HT composite.



**Figure 2.** Raman spectra of purified SWNTs, oxidized SWNTs, P3HT, and the SWNT-g-P3HT composite.



**Figure 3.** UV−visible spectra of (1) a SWNT film prepared with 0.4 mL of the SWNT suspension (31 mg·L$^{-1}$ in a SDS aqueous solution), and (2−7) the SWNT-g-P3HT composite films prepared by depositing various volumes of the SWNT-g-P3HT composite suspension (0.3, 0.6, 0.9, 1.2, 1.5, and 1.8 mL) on the top of the SWNT layer. The inset shows the change of the absorbance at 710 nm of the SWNT-g-P3HT composite films as a function of the volume of the composite suspension used.

solution). The SWNT film yields an optical absorption spectrum containing a peak at ca. 260 nm corresponding to the π-plasmon of SWNTs (curve 1 in Figure 3).[47] In the wavelength range of visible light, no resolved absorption peaks of SWNTs are detected because the SWNTs form bundles in the film. Upon deposition of a SWNT-g-P3HT composite layer on the top of the SWNT layer, an abroad peak is observed at ca. 530 nm, which corresponds to the optical absorption of P3HT (curves 2−7 in Figure 3). The absorption peak of P3HT is weak because of the low content of P3HT in the SWNT-g-P3HT composite (Figure 1a). The inset shows that the absorbance of the SWNT-g-P3HT composite films at 710 nm increases linearly with increasing the volume of the SWNT-g-
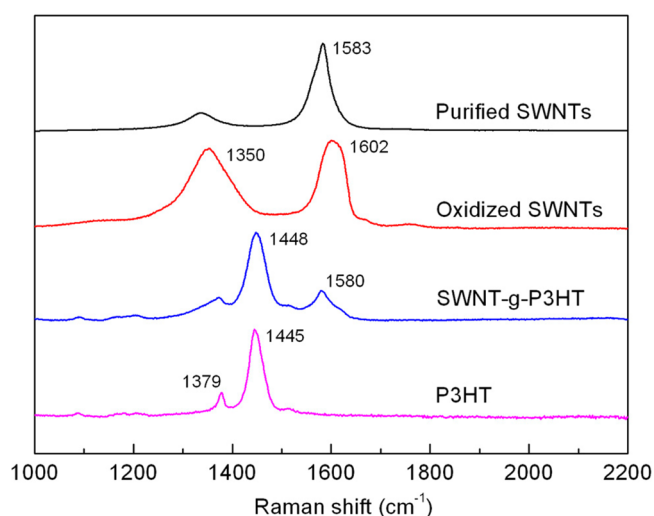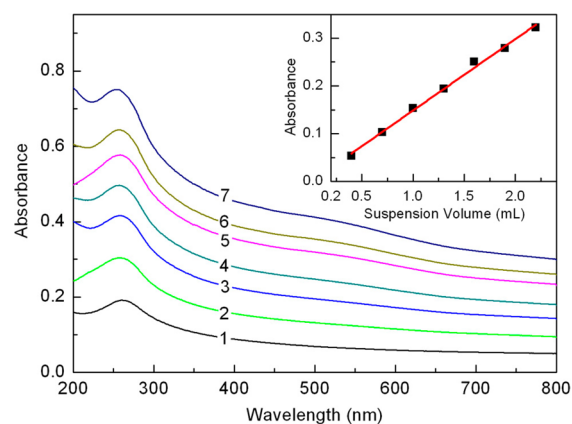
P3HT composite suspension. This result indicates that composite films of various thicknesses can be prepared by using different volumes of the SWNT-g-P3HT composite suspension.[32,35] The absorbance at 710 nm is used for evaluating the thickness of the films because the absorbance at this wavelength is solely ascribed to SWNTs.

Because the SWNT-g-P3HT composite films will be used as an electrochemical electrode, their electrical conductivity is an important parameter. Figure 4 summarizes the sheet resistance of the SWNT film and the SWNT-g-P3HT composite films. The SWNT film has a transparency of 89% (point 1 in Figure 4), which is on the conductive side of the percolation threshold.[48] Thus, such a SWNT layer is capable of supporting the SWNT-g-P3HT composite layer. Upon deposition of a SWNT-g-P3HT composite layer (0.3 mL of the SWNT-g-P3HT composite suspension), the sheet resistance of the composite film is increased (point 2 in Figure 4). This is due to the fact that the sheet resistance of the SWNT-g-P3HT composite layer is higher than that of the SWNT layer because
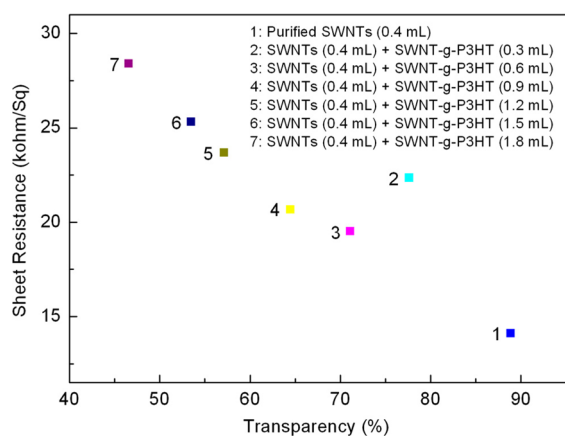
7689

dx.doi.org/10.1021/am500973m | ACS Appl. Mater. Interfaces 2014, 6, 7686−7694

**Figure 4.** Relationship between the sheet resistance and the transparency at 710 nm of the SWNT-g-P3HT composite films.

of two factors: (1) the deteriorated conductivity of the SWNTs because of the altered electronic properties during the covalent grafting, (2) the isolating effect of the P3HT attached on the surfaces of SWNTs. When the volume of the SWNT-g-P3HT composite suspension (0.6 mL) is increased, the sheet resistance of the resultant film is decreased because the SWNT-g-P3HT composite forms a continuous network in its own layer (point 3 in Figure 4). When the volume of the SWNT-g-P3HT composite suspension is further increased, the sheet resistance of the corresponding films is gradually increased because the isolating effect of the P3HT grafted (points 4, 5, 6, and 7 in Figure 4). These experiments were repeated and the results were reproducible, indicating that the observed changing tendency of the sheet resistance of the SWNT-g-P3HT composite films is reliable. Because we use the SWNT-g-P3HT composite films as an electrochemical electrode as discussed below, it is important to choose a film that has relatively lower sheet resistance.

To further investigate the SWNT-g-P3HT composite films, SEM was used to observe their morphologies. Figure 5 displays
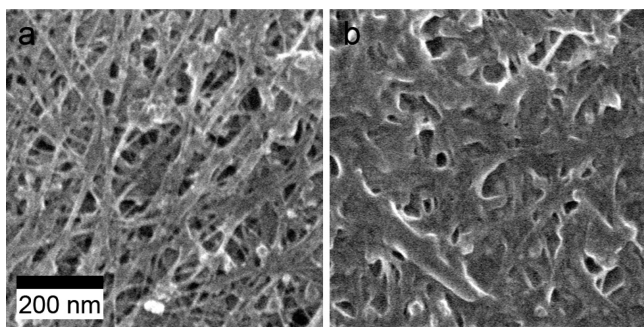


**Figure 5.** SEM images of (a) the SWNT film and (b) the SWNT-g-P3HT composite film prepared with 0.4 mL of the purified SWNT suspension and 0.6 mL of the SWNT-g-P3HT composite suspension.

SEM images of the SWNT film and the SWNT-g-P3HT composite film prepared by using 0.4 mL of the purified SWNTs suspension and 0.6 mL of the SWNT-g-P3HT composite suspension. In the SEM image of the SWNT film (Figure 5a), one can see clear SWNT bundles. In contrast, in the SEM image of the SWNT-g-P3HT composite film (Figure 5b), the SWNT bundles are concealed by grafted P3HT. Such a

morphology feature confirms the explanation of the change of sheet resistance of the SWNT-g-P3HT composite films.

Because the SWNT-g-P3HT composite films are used as an electrochemical electrode, the films that have low sheet resistance are preferred. Thus, the SWNT-g-P3HT composite films prepared with 0.6 mL of SWNT-g-P3HT composite suspension were used for electrochemical detection of metal ions (point 3 in Figure 4). For electrochemical detection, glass carbon electrodes are commonly used.[29,30] However, the applications of glass carbon electrodes are handicapped by their high price and small size of the electrode tip. In contrast, our SWNT-g-P3HT composite electrodes are easily prepared and have a large size up to square centimeters. A large area of the electrode can significantly enhance the detection limitation. Figure 6a shows the CV curves of a bare ITO electrode, the
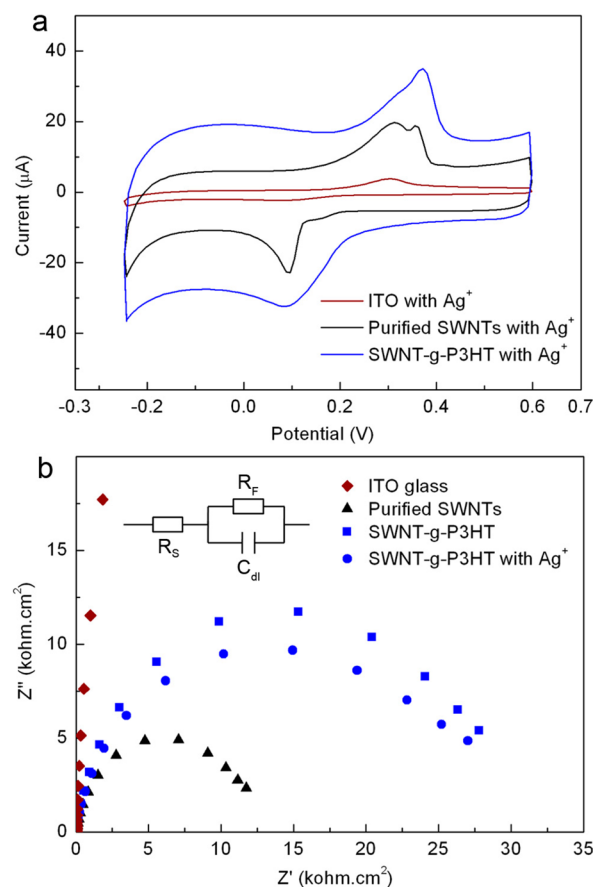


**Figure 6.** (a) CV curves of bare ITO electrode, the SWNT electrode, and the SWNT-g-P3HT composite electrode in the presence of $Ag^+$ ions ($AgNO_3$, 1 mg·$L^{-1}$ in aqueous solution), and (b) EIS curves of ITO electrode, the SWNT electrode, and the SWNT-g-P3HT composite electrode in the absence of $Ag^+$ ions, and the EIS curve of the SWNT-g-P3HT composite electrode in the presence of $Ag^+$ ions ($AgNO_3$, 1 mg·$L^{-1}$ in aqueous solution).

SWNT electrode, and the SWNT-g-P3HT composite electrode in the presence of $Ag^+$ ions ($AgNO_3$, 1 mg·$L^{-1}$ in aqueous solution). To avoid electrochemical degradation of P3HT,[49] a potential window from −0.25 to +0.6 V was chosen, where the oxidative/reductive peaks of P3HT did not appear (Figure S4, Supporting Information). The bare ITO electrode produces an oxidative peak at 0.34 V and a reductive peak at 0.07 V, which correspond to the oxidation/reduction process of Ag/$Ag^+$ species. For the SWNT electrode, the CV curve has three

features. First, both the oxidative peak and the reductive peak become stronger, indicating that the redox reactions of Ag/Ag$^+$ are more likely to take place on the surfaces of SWNTs. This might be due to the fact that the Ag/Ag$^+$ species show more preferential interactions with SWNTs than with ITO. Second, the oxidative peak divides into two peaks that locate at 0.31 and 0.36 V. The dual-peak feature might be due to different local structures of the SWNT surfaces: $\pi$-conjugated structure and local defect structure. Third, the CV curve appears a wider loop than the CV curve of the ITO electrode. This finding can be ascribed to the capacitive characteristic of SWNTs.[50,51] Significantly, the SWNT-g-P3HT composite electrode generates a CV curve that has the widest loop and the strongest oxidative/reductive peaks among the three electrodes. The further widened loop of the CV curve could be attributed to the combined capacitive characteristic of SWNTs and P3HT.[52] And the enhanced electrochemical response of Ag/Ag$^+$ species to the SWNT-g-P3HT electrode can be interpreted as complexation interactions of Ag/Ag$^+$ species with the sulfur atoms in P3HT,[49,53] as pristine P3HT shows electrochemical response in detection of Ag$^+$ ions.[54] And as a result, the dual-peak feature is not as resolved as that of the SWNT electrode. In addition, for the CV curves of both the SWNT electrode and the SWNT-g-P3HT electrode, the left side is wider than the right side. This is due to the influence of the supporting electrolyte (KNO$_3$). In a control experiment, a SWNT/P3HT composite film was also prepared by casting P3HT on the surface of a SWNT film (Figure S5, Supporting Information). The oxidative/reductive peaks of the Ag/Ag$^+$ species by using the SWNT/P3HT composite electrode are weaker than by using the SWNT-g-P3HT composite electrode. This might be due to the fact that the interfacial interaction between SWNTs and P3HT in the SWNT/P3HT composite is not as intimate as in the SWNT-g-P3HT composite.

To further investigate the electrochemical characteristic of these different electrodes, EIS measurement was performed (Figure 6b). An ITO electrode shows a linear relationship between Z″ and Z′ in the complex plane, whereas the SWNT electrode and the SWNT-g-P3HT composite electrode display semicircles of the Z″ vs Z′ complex-plane plots. These results also indicate that the SWNT electrode and the SWNT-g-P3HT composite electrode have capacitive feature. The diameter of the semicircle for the SWNT electrode is smaller than that for the SWNT-g-P3HT electrode, indicating that the interface resistance ($R_F$) between the electrochemical electrode and the supporting electrolyte is smaller for the SWNT electrode than for the SWNT-g-P3HT composite electrode. The $R_F$ can be obtained through fitting the experimental data by following the model shown in the inset of Figure 6b. As a result, the $R_F$ values were obtained to be 10.1 and 23.8 kohm·cm$^2$ for the SWNT electrode and for the SWNT-g-P3HT composite electrode, respectively. The enlarged $R_F$ for the SWNT-g-P3HT composite electrode might be due to the isolating effect of the P3HT grafted on the surface of SWNTs (Figures 1c and 5b). On the other hand, the diameter of the semicircle for the SWNT-g-P3HT composite electrode becomes smaller upon addition of Ag$^+$ ions into the testing solution: the $R_F$ was obtained to be 21.7 kohm·cm$^2$. The decreased $R_F$ could be ascribed to the complexation interactions between Ag/Ag$^+$ species and the sulfur atoms in P3HT. Thus, the EIS curves of the different electrodes provide interface information between the electrode, electrolyte, and Ag$^+$ ions, which explains

the enhanced electrochemical detection of Ag$^+$ ions by using the SWNT-g-P3HT composite electrode.

Quantitative detection is essential for detection technique. Figure 7a shows the CV curves of the SWNT-g-P3HT
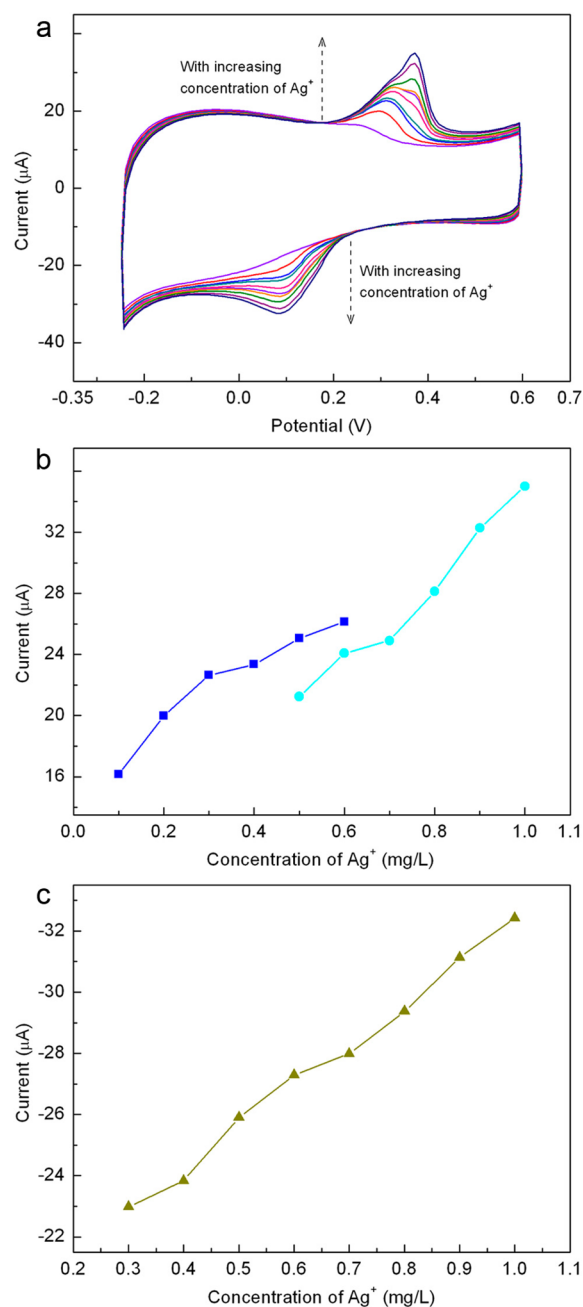


**Figure 7.** (a) CV curves of the SWNT-g-P3HT composite electrode at various concentrations of Ag$^+$ ions (AgNO$_3$, from 0.1 to 1 mg·L$^{-1}$ in aqueous solution), (b) intensity changes of the oxidative peaks at the low-potential (solid square) and at the high-potential (solid dot) as a function of the concentration of Ag$^+$ ions, and (c) intensity change of the reductive peak as a function of the concentration of Ag$^+$ ions.

composite electrode in the presence of various concentrations of Ag$^+$ ions: From 0.1 to 1 mg·L$^{-1}$ of AgNO$_3$ in aqueous solution. It is seen that the intensities of both the oxidative peak and the reductive peak increase with increasing the concentration of Ag$^+$ ions. In this process, the low-potential oxidative peak becomes indistinct and the high-potential

oxidative peak appears dominated. The current values of the oxidative/reductive peaks were plotted as a function of the concentration of $AgNO_3$. The electrochemical current of the oxidative peaks increases with increasing the concentration of $Ag^+$ ions (Figure 7b). On the other hand, the electrochemical current of the reduction peak increases linearly as a function of the concentration of $Ag^+$ ions (Figure 7c). These results indicate that the SWNT-g-P3HT composite electrode can be used for quantitative detection of $Ag^+$ ions. Notably, because the area of the SWNT-g-P3HT composite electrode is large up to square centimeters, it has a larger interface with the electrolyte than the traditional glassy carbon electrode. Thus, the detection limitation of $Ag^+$ ions can be as low as $0.1$ mg·L$^{-1}$ for $AgNO_3$ (Figure S6, Supporting Information), which is lower than the values of previous reports.[54]

Selective detection is another essential factor for detection technique. In this work, we tried most commonly used transition metal ions, including $Cr^{3+}$ ($Cr(NO_3)_3$·$9H_2O$, $E^\theta = -0.74$ V), $Fe^{2+}$ ($FeCl_2$·$4H_2O$, $E^\theta = -0.44$ V), $Fe^{3+}$ ($Fe(NO_3)_3$·$9H_2O$, $E^\theta = -0.04$ V), $Co^{2+}$ ($Co(NO_3)_2$·$6H_2O$, $E^\theta = -0.28$ V), $Ni^{2+}$ ($Ni(NO_3)_2$·$6H_2O$, $E^\theta = -0.25$ V), $Cu^{2+}$ ($Cu(NO_3)_2$·$3H_2O$, $E^\theta = +0.34$ V), $Zn^{2+}$ ($Zn(NO_3)_2$·$6H_2O$, $E^\theta = -0.7618$ V), $Pb^{2+}$ ($Pb(NO_3)_2$, $E^\theta = -0.13$ V), $Ag^+$ ($AgNO_3$, $E^\theta = +0.7996$ V), $Cd^{2+}$ ($Cd(NO_3)_2$·$4H_2O$, $E^\theta = -0.4$ V), and $Hg^{2+}$ ($Hg(NO_3)_2$·$H_2O$, $E^\theta = +0.85$ V) (in the brackets are displayed the salts used for tests and the standard electrode potentials of the corresponding metal ions relative to the standard hydrogen electrode). According to the standard electrode potentials of these ions, one can expect that only $Ag/Ag^+$ and $Hg/Hg^{2+}$ species show oxidative/reductive peaks in the scanned potential window (from $-0.25$ to $+0.6$ V). Such speculation has been confirmed by experimental data. An oxidative peak appeared at ca. $0.41$ V in the CV curves of a $Hg(NO_3)_2$·$H_2O$ aqueous solution ($1$ mg·L$^{-1}$) (Figure S7, Supporting Information), whereas no oxidative/reductive peaks were detected for the other metal ions in the potential window from $-0.25$ to $+0.6$ V (not shown). It is seen that the SWNT-g-P3HT composite electrode does not generate stronger oxidative/reductive peaks than the SWNT electrode. This might be due to the fact that the synergic effect of electrocatalytic properties from SWNTs and P3HT is not optimized at the component ratio for the SWNT-g-P3HT composite. Furthermore, the potential value of the oxidation peak of $Hg^{2+}$ ions is higher than that of $Ag^+$ ions: $0.41$ V for the former and $0.31$ and $0.34$ V for the latter. Therefore, $Ag^+$ and $Hg^{2+}$ ions can be differentiated by using the SWNT-g-P3HT composite electrode in this electrochemical detection. In addition, because this detection technique depends on the standard electrode potentials of the metal ions and the preferential interactions of the metal ions with the electrode material, the SWNT-g-P3HT composite electrode shows a marked advantage in selective detection.

## CONCLUSIONS

A SWNT-g-P3HT composite was prepared through covalently grafting P3HT on the surfaces of SWNTs. TEM observation and Raman spectra of the composite indicated intimate interactions between SWNTs and P3HT in the composite. The SWNT-g-P3HT composite films were prepared by using a modified vacuum-assisted deposition approach, in which the SWNT-g-P3HT composite was deposited on the top of a SWNT layer. The optical and electrical properties of the SWNT-g-P3HT composite films could be controlled by changing the volumes of the SWNT-g-P3HT composite

suspension used. Due to complexation interactions of $Ag^+$ ions with the sulfur atoms in P3HT, the SWNT-g-P3HT composite films prepared on an ITO substrate showed selective and quantitative detection of $Ag^+$ ions among commonly used transition metal ions. Finally, the SWNT-g-P3HT composite films show advantages in simple and large-sized preparation; as a result, the SWNT-g-P3HT composite electrode exhibited enhanced limitation for electrochemical detection of $Ag^+$ ions.

## ASSOCIATED CONTENT

### Ⓢ Supporting Information

Synthesis of amino-terminated poly(3-hexylthiophene), FT-IR spectra of the products in the synthesis of the SWNT-g-P3HT composite, and additional electrochemical characterization. This material is available free of charge via the Internet at http://pubs.acs.org.

## AUTHOR INFORMATION

### Corresponding Author

*J. Geng. E-mail: jianxingeng@mail.ipc.ac.cn.

### Author Contributions

#Equal contribution to this work.

### Notes

The authors declare no competing financial interest.

## REFERENCES

(1) Han, K. N.; Li, C. A.; Bui, M.-P. N.; Seong, G. H. Patterning of Single-Walled Carbon Nanotube Films on Flexible, Transparent Plastic Substrates. *Langmuir* **2010**, *26*, 598−602.

(2) Wu, Z. C.; Chen, Z. H.; Du, X.; Logan, J. M.; Sippel, J.; Nikolou, M.; Kamaras, K.; Reynolds, J. R.; Tanner, D. B.; Hebard, A. F.; Rinzler, A. G. Transparent, Conductive Carbon Nanotube Films. *Science* **2004**, *305*, 1273−1276.

(3) Okimoto, H.; Takenobu, T.; Yanagi, K.; Miyata, Y.; Shimotani, H.; Kataura, H.; Iwasa, Y. Tunable Carbon Nanotube Thin-Film Transistors Produced Exclusively via Inkjet Printing. *Adv. Mater.* **2010**, *22*, 3981−3986.

(4) Choi, Y. S.; Sung, J.; Kang, S. J.; Cho, S. H.; Hwang, I.; Hwang, S. K.; Huh, J.; Kim, H.-C.; Bauer, S.; Park, C. Control of Current Hysteresis of Networked Single-Walled Carbon Nanotube Transistors by a Ferroelectric Polymer Gate Insulator. *Adv. Funct. Mater.* **2013**, *23*, 1120−1128.

(5) Lau, P. H.; Takei, K.; Wang, C.; Ju, Y.; Kim, J.; Yu, Z.; Takahashi, T.; Cho, G.; Javey, A. Fully Printed, High Performance Carbon Nanotube Thin-Film Transistors on Flexible Substrates. *Nano Lett.* **2013**, *13*, 3864−3869.

(6) Li, W.-S.; Hou, P.-X.; Liu, C.; Sun, D.-M.; Yuan, J.; Zhao, S.-Y.; Yin, L.-C.; Cong, H.; Cheng, H.-M. High-Quality, Highly Concentrated Semiconducting Single-Wall Carbon Nanotubes for Use in Field Effect Transistors and Biosensors. *ACS Nano* **2013**, *7*, 6831−6839.

(7) Lipomi, D. J.; Vosgueritchian, M.; Tee, B. C. K.; Hellstrom, S. L.; Lee, J. A.; Fox, C. H.; Bao, Z. Skin-Like Pressure and Strain Sensors Based on Transparent Elastic Films of Carbon Nanotubes. *Nat. Nanotechnol.* **2011**, *6*, 788−792.

(8) Roberts, M. E.; LeMieux, M. C.; Bao, Z. Sorted and Aligned Single-Walled Carbon Nanotube Networks for Transistor-Based Aqueous Chemical Sensors. *ACS Nano* **2009**, *3*, 3287–3293.

(9) Zhang, D.; Ryu, K.; Liu, X.; Polikarpov, E.; Ly, J.; Tompson, M. E.; Zhou, C. Transparent, Conductive, and Flexible Carbon Nanotube Films and Their Application in Organic Light-Emitting Diodes. *Nano Lett.* **2006**, *6*, 1880–1886.

(10) Yang, S. B.; Kong, B. S.; Geng, J.; Jung, H. T. Enhanced Electrical Conductivities of Transparent Double-Walled Carbon Nanotube Network Films by Post-treatment. *J. Phys. Chem. C* **2009**, *113*, 13658–13663.

(11) Wang, C.; Takei, K.; Takahashi, T.; Javey, A. Carbon Nanotube Electronics - Moving forward. *Chem. Soc. Rev.* **2013**, *42*, 2592–2609.

(12) Takahashi, T.; Takei, K.; Gillies, A. G.; Fearing, R. S.; Javey, A. Carbon Nanotube Active-Matrix Backplanes for Conformal Electronics and Sensors. *Nano Lett.* **2011**, *11*, 5408–5413.

(13) Wang, C.; Chien, J.-C.; Takei, K.; Takahashi, T.; Nah, J.; Niknejad, A. M.; Javey, A. Extremely Bendable, High-Performance Integrated Circuits Using Semiconducting Carbon Nanotube Networks for Digital, Analog, and Radio-Frequency Applications. *Nano Lett.* **2012**, *12*, 1527–1533.

(14) Green, A. A.; Hersam, M. C. Colored Semitransparent Conductive Coatings Consisting of Monodisperse Metallic Single-Walled Carbon Nanotubes. *Nano Lett.* **2008**, *8*, 1417–1422.

(15) Blackburn, J. L.; Barnes, T. M.; Beard, M. C.; Kim, Y.-H.; Tenent, R. C.; McDonald, T. J.; To, B.; Coutts, T. J.; Heben, M. J. Transparent Conductive Single-Walled Carbon Nanotube Networks with Precisely Tunable Ratios of Semiconducting and Metallic Nanotubes. *ACS Nano* **2008**, *2*, 1266–1274.

(16) Lu, F.; Wang, W.; Fernando, K. A. S.; Meziani, M. J.; Myers, E.; Sun, Y.-P. Metallic Single-Walled Carbon Nanotubes for Transparent Conductive Films. *Chem. Phys. Lett.* **2010**, *497*, 57–61.

(17) Geng, H.-Z.; Kim, K. K.; So, K. P.; Lee, Y. S.; Chang, Y.; Lee, Y. H. Effect of Acid Treatment on Carbon Nanotube-Based Flexible Transparent Conducting Films. *J. Am. Chem. Soc.* **2007**, *129*, 7758–7759.

(18) Shim, D.; Jung, S.-H.; Han, S. Y.; Shin, K.; Lee, K.-H.; Han, J. H. Improvement of SWCNT Transparent Conductive Films via Transition Metal Doping. *Chem. Commun.* **2011**, *47*, 5202–5204.

(19) Park, S. H.; Jin, S. H.; Jun, G. H.; Jeon, S.; Hong, S. H. Enhanced Electrical Properties in Carbon Nanotube/Poly (3-hexylthiophene) Nanocomposites Formed through Non-Covalent Functionalization. *Nano Res.* **2011**, *4*, 1129–1135.

(20) Star, A.; Stoddart, J. F.; Steuerman, D.; Diehl, M.; Boukai, A.; Wong, E. W.; Yang, X.; Chung, S. W.; Choi, H.; Heath, J. R. Preparation and Properties of Polymer-Wrapped Single-Walled Carbon Nanotubes. *Angew. Chem., Int. Ed.* **2001**, *40*, 1721–1725.

(21) Chen, J.; Liu, H. Y.; Weimer, W. A.; Halls, M. D.; Waldeck, D. H.; Walker, G. C. Noncovalent Engineering of Carbon Nanotube Surfaces by Rigid, Functional Conjugated Polymers. *J. Am. Chem. Soc.* **2002**, *124*, 9034–9035.

(22) Ikeda, A.; Nobusawa, K.; Hamano, T.; Kikuchi, J. Single-Walled Carbon Nanotubes Template the One-Dimensional Ordering of a Polythiophene Derivative. *Org. Lett.* **2006**, *8*, 5489–5492.

(23) Park, H. S.; Choi, B. G.; Hong, W. H.; Jang, S.-Y. Interfacial Interactions of Single-Walled Carbon Nanotube/Conjugated Block Copolymer Hybrids for Flexible Transparent Conductive Films. *J. Phys. Chem. C* **2012**, *116*, 7962–7967.

(24) Sung, J.; Huh, J.; Choi, J.-H.; Kang, S. J.; Choi, Y. S.; Lee, G. T.; Cho, J.; Myoung, J.-M.; Park, C. Ultrathin Electronic Composite Sheets of Metallic/Semiconducting Carbon Nanotubes Embedded in Conjugated Block Copolymers. *Adv. Funct. Mater.* **2010**, *20*, 4305–4313.

(25) Sung, J.; Choi, Y. S.; Kang, S. J.; Cho, S. H.; Lee, T.-W.; Park, C. AC Field-Induced Polymer Electroluminescence with Single Wall Carbon Nanotubes. *Nano Lett.* **2011**, *11*, 966–972.

(26) Kuila, B. K.; Park, K.; Dai, L. Soluble P3HT-Grafted Carbon Nanotubes: Synthesis and Photovoltaic Application. *Macromolecules* **2010**, *43*, 6699–6705.

(27) Geng, J. X.; Kong, B. S.; Yang, S. B.; Youn, S. C.; Park, S.; Joo, T.; Jung, H. T. Effect of SWNT Defects on the Electron Transfer Properties in P3HT/SWNT Hybrid Materials. *Adv. Funct. Mater.* **2008**, *18*, 2659–2665.

(28) Geng, J. X.; Zeng, T. Y. Influence of Single-Walled Carbon Nanotubes Induced Crystallinity Enhancement and Morphology Change on Polymer Photovoltaic Devices. *J. Am. Chem. Soc.* **2006**, *128*, 16827–16833.

(29) Hu, Y.; Zhao, Z.; Wan, Q. Facile Preparation of Carbon Nanotube-Conducting Polymer Network for Sensitive Electrochemical Immunoassay of Hepatitis B Surface Antigen in Serum. *Bioelectrochemistry* **2011**, *81*, 59–64.

(30) Qi, H.; Ling, C.; Huang, R.; Qiu, X.; Li, S.; Gao, Q.; Zhang, C. Functionalization of Single-Walled Carbon Nanotubes with Protein by Click Chemistry as Sensing Platform for Sensitized Electrochemical Immunoassay. *Electrochim. Acta* **2012**, *63*, 76–82.

(31) Smithson, C. S.; Zhu, S.; Wigglesworth, T.; Wu, Y. Unsorted Single Walled Carbon Nanotubes Enabled the Fabrication of High Performance Organic Thin Film Transistors with Low Cost Metal Electrodes. *Chem. Commun.* **2013**, *49*, 8791–8793.

(32) Zhao, W.; Tong, B.; Shi, J.; Pan, Y.; Shen, J.; Zhi, J.; Chan, W. K.; Dong, Y. Fabrication and Optoelectronic Properties of Novel Films Based on Functionalized Multiwalled Carbon Nanotubes and (Phthalocyaninato)Ruthenium(II) via Coordination Bonded Layer-by-Layer Self-Assembly. *Langmuir* **2010**, *26*, 16084–16089.

(33) Sarker, B. K.; Arif, M.; Khondaker, S. I. Near-Infrared Photoresponse in Single-Walled Carbon Nanotube/Polymer Composite Films. *Carbon* **2010**, *48*, 1539–1544.

(34) Sun, X.; Zhang, Z.; Lu, X.; Guan, G.; Li, H.; Peng, H. Electric Current Test Paper Based on Conjugated Polymers and Aligned Carbon Nanotubes. *Angew. Chem., Int. Ed.* **2013**, *52*, 7776–7780.

(35) Pan, Y.; Tong, B.; Shi, J.; Zhao, W.; Shen, J.; Zhi, J.; Dong, Y. Fabrication, Characterization, and Optoelectronic Properties of Layer-by-Layer Films Based on Terpyridine-Modified MWCNTs and Ruthenium(III) Ions. *J. Phys. Chem. C* **2010**, *114*, 8040–8047.

(36) Yang, H.; Zhang, Q.; Shan, C.; Li, F.; Han, D.; Niu, L. Stable, Conductive Supramolecular Composite of Graphene Sheets with Conjugated Polyelectrolyte. *Langmuir* **2010**, *26*, 6708–6712.

(37) Casagrande, T.; Imin, P.; Cheng, F.; Botton, G. A.; Zhitomirsky, I.; Adronov, A. Synthesis and Electrophoretic Deposition of Single-Walled Carbon Nanotube Complexes with a Conjugated Polyelectrolyte. *Chem. Mater.* **2010**, *22*, 2741–2749.

(38) Reddy, B. N.; Deepa, M. Unraveling Nanoscale Conduction and Work Function in a Poly(3,4-ethylenedioxypyrrole)/Carbon Nanotube Composite by Kelvin Probe Force Microscopy and Conducting Atomic Force Microscopy. *Electrochim. Acta* **2012**, *70*, 228–240.

(39) Liu, C.; Cong, H. T.; Li, F.; Tan, P. H.; Cheng, H. M.; Lu, K.; Zhou, B. L. Semi-Continuous Synthesis of Single-Walled Carbon Nanotubes by a Hydrogen Arc Discharge Method. *Carbon* **1999**, *37*, 1865–1868.

(40) Chiang, I. W.; Brinson, B. E.; Huang, A. Y.; Willis, P. A.; Bronikowski, M. J.; Margrave, J. L.; Smalley, R. E.; Hauge, R. H. Purification and Characterization of Single-Wall Carbon Nanotubes (SWNTs) Obtained From the Gas-Phase Decomposition of CO (HiPco Process). *J. Phys. Chem. B* **2001**, *105*, 8297–8301.

(41) Jeffries-El, M.; Sauve, G.; McCullough, R. D. Facile Synthesis of End-Functionalized Regioregular Poly(3-alkylthiophene)s via Modified Grignard Metathesis Reaction. *Macromolecules* **2005**, *38*, 10346–10352.

(42) Geng, J.; Jung, H. Porphyrin Functionalized Graphene Sheets in Aqueous Suspensions: From the Preparation of Graphene Sheets to Highly Conductive Graphene Films. *J. Phys. Chem. C* **2010**, *114*, 8227–8234.

(43) Geng, J.; Liu, L. J.; Yang, S. B.; Youn, S. C.; Kim, D. W.; Lee, J. S.; Choi, J. K.; Jung, H. T. A Simple Approach for Preparing Transparent Conductive Graphene Films Using the Controlled Chemical Reduction of Exfoliated Graphene Oxide in an Aqueous Suspension. *J. Phys. Chem. C* **2010**, *114*, 14433–14440.

(44) Jeong, S. H.; Kim, K. K.; Jeong, S. J.; An, K. H.; Lee, S. H.; Lee, Y. H. Optical Absorption Spectroscopy for Determining Carbon Nanotube Concentration in Solution. *Synth. Met.* **2007**, *157*, 570−574.

(45) Chunder, A.; Liu, J. H.; Zhai, L. Reduced Graphene Oxide/Poly(3-hexylthiophene) Supramolecular Composites. *Macromol. Rapid Commun.* **2010**, *31*, 380−384.

(46) Meng, D.; Sun, J.; Jiang, S.; Zeng, Y.; Li, Y.; Yan, S.; Geng, J.; Huang, Y. Grafting P3HT Brushes on GO Sheets: Distinctive Properties of the GO/P3HT Composites due to Different Grafting Approaches. *J. Mater. Chem.* **2012**, *22*, 21583−21591.

(47) Pichler, T.; Knupfer, M.; Golden, M. S.; Fink, J.; Rinzler, A.; Smalley, R. E. Localized and Delocalized Electronic States in Single-Wall Carbon Nanotubes. *Phys. Rev. Lett.* **1998**, *80*, 4729−4732.

(48) Hu, L.; Hecht, D. S.; Gruner, G. Percolation in Transparent and Conducting Carbon Nanotube Networks. *Nano Lett.* **2004**, *4*, 2513−2517.

(49) Song, F. Y.; Shiu, K. K. Preconcentration and Electroanalysis of Silver Species at Polypyrrole Film Modified Glassy Carbon Electrodes. *J. Electroanal. Chem.* **2001**, *498*, 161−170.

(50) Feng, G.; Li, S.; Atchison, J. S.; Presser, V.; Cummings, P. T. Molecular Insights into Carbon Nanotube Supercapacitors: Capacitance Independent of Voltage and Temperature. *J. Phys. Chem. C* **2013**, *117*, 9178−9186.

(51) Futaba, D. N.; Hata, K.; Yamada, T.; Hiraoka, T.; Hayamizu, Y.; Kakudate, Y.; Tanaike, O.; Hatori, H.; Yumura, M.; Iijima, S. Shape-Engineerable and Highly Densely Packed Single-Walled Carbon Nanotubes and Their Application as Super-Capacitor Electrodes. *Nat. Mater.* **2006**, *5*, 987−994.

(52) Gnanakan, S. R. P.; Rajasekhar, M.; Subramania, A. Synthesis of Polythiophene Nanoparticles by Surfactant-Assisted Dilute Polymerization Method for High Performance Redox Supercapacitors. *Int. J. Electrochem. Sci.* **2009**, *4*, 1289−1301.

(53) Jimenez-Morales, A.; Galvan, J. C.; Aranda, P. A New Silver-Ion Selective Sensor Based on A Polythiacrown-Ether Entrapped by Sol-Gel. *Electrochim. Acta* **2002**, *47*, 2281−2287.

(54) Zejli, H.; de Cisneros, J. L. H.-H.; Naranjo-Rodriguez, I.; Temsamani, K. R. Stripping Voltammetry of Silver Ions at Polythiophene-Modified Platinum Electrodes. *Talanta* **2007**, *71*, 1594−1598.

7694

dx.doi.org/10.1021/am500973m | *ACS Appl. Mater. Interfaces* 2014, 6, 7686−7694